4. Ishida S, Matsumoto S, Yokoyama H, et al. An ESR-CT imaging of the head of a living rat receiving an administration of a nitroxide radical. *Magn Reson Imaging* 1992;10: 109–114.
5. Slivka A, Spina MB, Cohen G. Reduced and oxidized glutathione in human and monkey brain. *Neurosci Lett* 1987;74:112–118.
6. Sharp PF, Smith FW, Gemmell HG, et al. Technetium-99m-HMPAO stereoisomers as potential agents for imaging regional cerebral blood flow: human volunteer studies. *J Nucl Med* 1987;27:171–177.
7. Matsuda H, Oba H, Seki H, et al. Determination of flow and rate constants in a kinetic model of [^{99m}Tc]-hexamethyl-propyleneamine oxime in the human brain. *J Cereb Blood Flow Metabol* 1988;8:S61–S68.
8. Lassen NA, Andersen AR, Friberg L, Paulson OB. The retention of [^{99m}Tc]-*d,l*-HMPAO in the human brain after intracarotid bolus injection: a kinetic analysis. *J Cereb Blood Flow Metabol* 1988;8:S13–S22.
9. Ballinger JR, Reid RH, Gulenchyn KY. Technetium-99m-HMPAO stereoisomers: differences in interaction with glutathione. *J Nucl Med* 1988;29:1998–2000.
10. Neirinckx RD, Burke JF, Harrison RC, Forster AM, Andersen AR, Lassen NA. The retention mechanism of technetium-99m-HMPAO: intracellular reaction with glutathione. *J Cereb Blood Flow Metabol* 1988;8:S4–S12.
11. Andersen AR, Friberg H, Lassen NA, Kristensen K, Neirinckx RD. Assessment of the arterial input curve for [^{99m}Tc]-*d,l*-HMPAO by rapid octanol extraction. *ibid.* 1988; 8:S23–S30.
12. Neirinckx RD, Canning LR, Piper IM, et al. Technetium-99m d,l-HMPAO: a new radiopharmaceutical cerebral blood perfusion. *J Nucl Med* 1987;28:191–202.
13. Nowotnik DP, Canning LR, Cumming SA, et al. Development of a ^{99m}Tc-labeled radiopharmaceutical for cerebral blood flow imaging. *Nucl Med Commun* 1985;6:499–506.
14. Plummer JL, Smith BR, Sies H, Bend JR. Chemical depletion of glutathione in vivo. *Methods Enzymol* 1981;77:50–59.
15. Demaster EG, Shirota FN, Redfern B, Goon DJW, Nagasawa HT. Analysis of hepatic reduced glutathione, cysteine and homocysteine by cationе-exchange high-performance liquid chromatography with electrochemical detection. *J Chromatogr* 1984; 308:83–91.
16. Ellman GL. Tissue sulfhydryl groups. *Arch Biochem Biophys* 1959;82:70–77.
17. Marstein S, Jellum E, Nesbakken R, Perry TL. Biochemical investigations of biopsied brain tissue and autopsied organs from a patient with pyroglutamic acidemia (5-oxoprolinemia). *Clin Chim Acta* 1981;111:219–228.
18. Perry T, Yong VW. Idiopathic Parkinson's disease, progressive supranuclear palsy and glutathione metabolism in the substantia nigra of patients. *Neurosci Lett* 1986;67:269–274.
19. Boyne AF. A methodology for analysis of tissue sulfhydryl components. *Anal Biochem* 1972;46:639–653.
20. Cooper AJL, Pulsinelli WA, Duffy TE. Glutathione and ascorbate during ischemia and postischemic reperfusion in rat brain. *J Neurochem* 1980;35:1242–1245.
21. Rehncrona S, Folbergrova J, Smith DS, Siesjo BK. Influence of complete and pronounced incomplete cerebral ischemia and subsequent recirculation on cortical concentrations of oxidized and reduced glutathione in the rat. *J Neurochem* 1980;34: 477–486.
22. Slivka A, Cohen G. Brain ischemia markedly elevates levels of the neurotoxic amino acid, cysteine. *Brain Res* 1993;608:33–37.
23. Perry TL, Godin DV, Hansen S. Parkinson's disease: a disorder due to nigral glutathione deficiency? *Neurosci Lett* 1982;33:305–310.
24. Riederer P, Sofic E, Rausch W-D, et al. Transition metals, ferritin, glutathione and ascorbic acid in parkinsonian brains. *J Neurochem* 1989;52:515–520.

Coronary Flow and Flow Reserve by PET Simplified for Clinical Applications Using Rubidium-82 or Nitrogen-13-Ammonia

Katsuya Yoshida, Nizar Mullani and K. Lance Gould

Diagnostic Imaging Research, National Institute of Radiological Sciences, Chiba, Japan; and Positron Diagnostic Research Center and Division of Cardiology, Department of Medicine, University of Texas Medical School, Houston, Texas

To validate routine, noninvasive determination of absolute myocardial perfusion and coronary flow reserve (CFR), cardiac PET was performed in animals using a simplified imaging protocol, high-dose dipyridamole and a simplified quantitative algorithm specific for ^{82}Rb and ^{13}N-ammonia. **Methods:** One hundred thirty-five PET scans were obtained in eight dogs after intravenous ^{13}N-ammonia or ^{82}Rb using serial dynamic PET or a simple two-image dataset. A simple flow model using the two-image dataset was developed for each radionuclide to account for varying arterial input function, flow-dependent myocardial extraction and increased permeability surface area (PS) product due to capillary recruitment at high flows not incorporated into previous models. Myocardial perfusion by the simple model was compared to standard, complete, two-compartment kinetic models validated by comparison to electromagnetic flow meter. **Results:** For ^{13}N-ammonia, myocardial perfusion by the simple PET model correlated with that by complete compartmental analysis of multiple serial PET images with r = 0.94, slope = 0.96; CFR by compartmental analysis correlated with CFR by electromagnetic flow meter with r = 0.94, slope = 0.97. For ^{82}Rb, myocardial perfusion determined by the simple model correlated with that determined by complete compartmental analysis of multiple serial PET images with r = 0.98, slope = 1.06; CFR determined by compartmental analysis correlated with CFR by electromagnetic flow meter with r = 0.88, slope = 1.13. **Conclusion:** A simplified PET protocol using ^{13}N-ammonia or ^{82}Rb and simple flow models provide noninvasive measurement of CFR up to six times baseline flow throughout the heart and diagnostic image quality for routine clinical application.

Received Oct. 24,1994; revision accepted Dec. 13, 1995.

For correspondence or reprints contact: K. Lance Gould, MD, Professor of Medicine, University of Texas Medical School, MSB 4.258, 6431 Fannin St., Houston, TX 77030.

Key Words: PET; rubidium-82; nitrogen-13-ammonia; coronary flow reserve

J Nucl Med 1996; 37:1701-1712

Current pharmacologic or stress perfusion imaging reflects relative distribution of maximum coronary flow or relative coronary flow reserve (CFR) (*1,2*) which may be normal in the presence of diffuse or balanced coronary artery disease. However, absolute CFR, defined as maximum flow normalized to resting flow (*1,2*), is reduced by diffuse disease and therefore reflects its presence and severity. Based on a new approach for quantitative arteriographic analysis of the entire epicardial coronary arterial tree (*3,4*), we have demonstrated that patients with localized coronary artery stenoses have coronary arterial lumens that are diffusely 30% to 50% smaller than normal subjects (*3*).

Although multistenotic or diffuse coronary artery disease is common, there has been no clinical method of quantifying such disease or its cumulative fluid dynamic, functional severity. Intracoronary echocardiography may identify atherosclerosis in the wall of the coronary artery and reduced lumen size (*5*), but it is invasive and does not provide information on functional impairment of flow capacity. We have demonstrated the central role of PET in the comprehensive noninvasive management of coronary artery disease (*6–9*), particularly for changes in severity during reversal treatment (*7–9*). However, absolute coronary flow and flow reserve have not been routinely mea-

sured clinically due to complexity of flow models and poor quality of the brief serial images used for flow determinations.

Absolute CFR may be altered by large changes in heart rate and blood pressure in experimental animals (*1*) and in humans (*10*). However, the range of heart rate and blood pressure in resting, hemodynamically stable, supine humans is sufficiently narrow that measurements of CFR by Doppler catheter are reproducible with acceptable variability for clinical purposes (*10,11*). Current standard arteriographic or radionuclide technology does not measure absolute coronary flow or flow reserve. Since diffuse coronary artery disease is commonly present in addition to discrete stenoses, noninvasive measurement of myocardial flow or flow reserve regionally would be useful clinically for identifying and quantifying functional severity of and for after changes in its severity of diffuse or multistenosis coronary artery disease.

The most commonly used PET perfusion radionuclides for clinical applications are generator-produced ^{82}Rb and cyclotron-produced ^{13}N-ammonia. Accordingly, the purpose of this study was to validate experimentally a new PET protocol for measuring myocardial flow and flow reserve with simple analysis algorithms suitable for routine clinical use with these radionuclides while retaining diagnostic quality images.

MATERIALS AND METHODS

Animal Preparation

Eight conditioned mongrel dogs weighing an average of 27 kg were surgically prepared as previously reported from our laboratory (*1,2,4*). Briefly, dogs were anesthetized, intubated and ventilated with room air. Left thoractomy was performed and two Tygon/Teflon 20-gauge catheters were placed within the ascending aorta for pressure measurement and arterial blood collection. The dead space of these catheters was small (0.7–0.8 ml). To test experimental feasibility, acute experiments were performed in the first two dogs, and in six other dogs, chronic experiments were performed. A Zepta electromagnetic flow probe and a hydraulic cuff occluder were placed on the left circumflex coronary artery. After implantation of instruments, the wires and tubing were tunneled from the posterior chest and exited from the skin through separate stab wounds, with a 7-day postoperative recovery period before collecting PET data. All animals were treated humanely according to Helsinki guidelines and the study protocols were approved by the Animal Welfare Committee of the University of Texas Health Science Center.

PET Imaging Protocol

PET images were obtained using the University of Texas, nine-slice cesium fluoride tomograph with a reconstructed resolution of 12 mm FWHM as previously described (*12–14*). A transmission scan was obtained over 25–30 min containing 150 million counts using a ring of ^{68}Ga. As a 20-sec slow bolus, 5–10 mCi ^{13}N-ammonia or 8–15 mCi ^{82}Rb were injected intravenously in animals and 18–20 mCi ^{13}N-ammonia or 40–50 mCi ^{82}Rb in humans. Simultaneously with injection, data collection was begun for 2 min in list mode format followed by data collection in frame mode format for 5 min (^{82}Rb) or 15 min (^{13}N-ammonia). Rubidium-82 was obtained from a ^{82}Sr/^{82}Rb generator. Nitrogen-13-ammonia was prepared in the cyclotron of the University of Texas Medical School as previously described (*2,8,9,12,13–17*).

Blood Sampling

To compare arterial activity concentrations of ^{13}N and ^{82}Rb measured by well counting with those determined by PET in animals, serial blood samples were obtained from the aortic catheter at sampling intervals of 3–4 sec during the first minute and every 10 sec for the next minute. Each sample volume was 1–1.5 ml drawn by hand into a syringe over approximately 1–1.5 sec. Nitrogen-13 and ^{82}Rb activities were measured in a well counter and corrected for radioactive decay and well counter deadtime.

Experimental Protocols

After light sedation, dogs were positioned in right recumbency within the PET scanner and sedation was maintained using a combination of 1cc innovar i.m. and 2–4 cc pentobarbital i.v., repeated approximately every 2 hr. Hemodynamic data were recorded and coronary flow was measured. Before starting the PET scan, initial flow and pressure calibrations were made and baseline control recordings were obtained of the ECG, phasic coronary flow and aortic pressure. Coronary flow response was recorded after a 10-sec occlusion. Mechanical occlusion to check zero flow baseline for the electromagnetic flow meter was done at the beginning and end of each PET image at rest and after dipyridamole. After returning to baseline conditions, two rest PET scans followed by two to four dipyridamole scans were obtained for a total of four to six PET scans per experiment. Intravenous doses of dipyridamole ranged from 0.284 to 0.852 mg/kg given over 4 min to obtain a wide range of values of flow and arterial input function. An interval of at least 50 and 10 min, respectively, was used between each PET scan for ^{13}N-ammonia and ^{82}Rb to allow for physical decay of the isotopes. Thirty experiments consisting of 135 PET scans were obtained at rest and after varying doses of dipyridamole. Seventy-five of the PET scans were obtained with ^{13}N-ammonia and 60 with ^{82}Rb depending on generator availability. For different correlations within subsets of data, the number of datapoints (n) varied from 14 to 49 as shown on each graph subsequently.

Image Processing

Two-minute list mode data were processed as ten 6-sec images followed by six 10-sec images. A single image was also reconstructed using the first 1 min of data collection, beginning with the first rise of counts after intravenous injection. Single images were also reconstructed of the first 2 min of data collection (0–2 min) and of the second minute (1–2 min) of data. Arterial input function was obtained from a region of interest (ROI) in the left atrium which was clearly visible on 12–30-sec PET images after the injection to minimize partial volume spillover effects.

Deadtime losses were corrected empirically by calibrating the PET scanner using known activity in a phantom as described below. Temporal resolution of the PET scanner is software controlled to any time period, limited only by counting statistics.

To assess the feasibility of determining arterial input more simply from a single image, a left atrial ROI was also drawn on a single image of the blood pool on the 0–1-min and 0–2-min single images. The ROI size was 4–16 pixels, with each pixel representing 3 mm. To precisely locate myocardial activity measured by PET, myocardial ROIs were drawn on late myocardial images obtained in frame mode, and these ROIs were projected onto the serial 6- and 10-sec PET images and onto the 0–1-, 0–2- and 1–2-min single images.

Cross-Calibration between PET and Well Counter

To quantify radioactivity in blood and myocardium, three different devices were used: the PET scanner, a dose calibrator and a well counter. The dose calibrator was calibrated with National Bureau of Standards sources. The stability of the dose calibrator was checked by ^{60}Co and ^{137}Ce calibration sources two or three times per week; the observed variability was less than 1%. Therefore, we used the dose calibrator as a standard for calibrating the PET scanner. Cross-calibration of the PET scanner, well counter and dose calibrator was obtained using ^{82}Rb or ^{13}N-ammonia solution as follows: For these calibration factors, the reference activity was measured by the dose calibrator, diluted with

500 ml water and injected into a water-filled phantom 20 cm in diameter. A measured sample volume was counted from the phantom contents in the well counter. From the ratio of PET counts per minute per pixel to millicuries per milliliter in the dose calibrator, a PET-dose calibrator calibration factor for the PET scanner was derived for the cylindrical 20-cm phantom containing a solution of ^{82}Rb or ^{13}N-ammonia. From the ratio of counts per second per volume in the well counter to millicuries per milliliter in the dose calibrator, a dose calibrator-well counter calibration factor was also calculated. The fluctuations of the PET and well counter cross-calibration factors to the dose calibrator were less than 3% and 6%, respectively. The calibration factor of ^{82}Rb was slightly different from that of ^{13}N due to the different energy spectrum between ^{13}N and ^{82}Rb, especially in the high energy range caused by the beta particle (3.15 MeV) of ^{82}Rb, which affected the integral value measured by the well counter. Therefore, we used a separate calibration factor for ^{82}Rb and ^{13}N.

Mathematical Basis of Myocardial Blood Flow Calculations

To measure perfusion using radionuclides extracted by the myocardium, simple flow models for ^{82}Rb and ^{13}N-ammonia were developed, using the following equation as a starting point (*15–17*):

$$E \cdot F = \frac{P(t)}{\int_0^t Ca(x)\,dx},$$

where P(t) is tracer uptake in an organ after time t, Ca(x) dx is the arterial blood concentration, F is coronary perfusion, E is the myocardial extraction fraction of the tracer, and in this form of the equation, x, is an integration "dummy." The advantage of this model is physiologic relevance to known microvascular spaces and kinetic-behavior of potassium or potassium analogs (*15–23*), its simplicity and applicability for routine clinical use. However, extraction fraction is not constant for all flow values but is a complex function of flow and of the permeability-surface area product of the capillary. Arterial input function is variable, depending on the effects of dipyridamole as shown subsequently. This simple model is not related to or dependent on the first-pass transit time of radiotracer.

As reference standards for comparison to our simple method, several compartmental models for ^{13}N-ammonia and ^{82}Rb have been validated for quantifying myocardial perfusion by curve fitting equations of the model to observed time-activity curves from multiple serial PET images to solve for multiple unknowns of compartmental models (*15,24–31*). Therefore, we compared myocardial perfusion measured by the simple models to standard compartmental models for both ^{82}Rb and ^{13}N-ammonia, which were adapted to account for increased PS product occurring at high flows after dipyridamole. As further validation, CFR calculated with these compartmental models for both radionuclides was compared to CFR obtained by electromagnetic flow meter to verify their validity and applicability as a PET reference standard.

For clinical application of either the simple flow models or complete compartmental models, noninvasive measurement of integrated arterial input function is needed. Cardiac PET can provide noninvasive measurement of arterial input function from ROIs drawn over the left ventricular cavity or the left atrium from multiple serial 6–10-sec images. Since dipyridamole increases cardiac output, it should theoretically decrease the integrated arterial input function below resting values, but the effect of dipyridamole on arterial input has not been reported, especially for high-dose dipyridamole. Therefore, we also compared arterial input function measured by blood sampling data with that measured noninvasively by PET and evaluated the effect of dipyridamole on arterial input function.

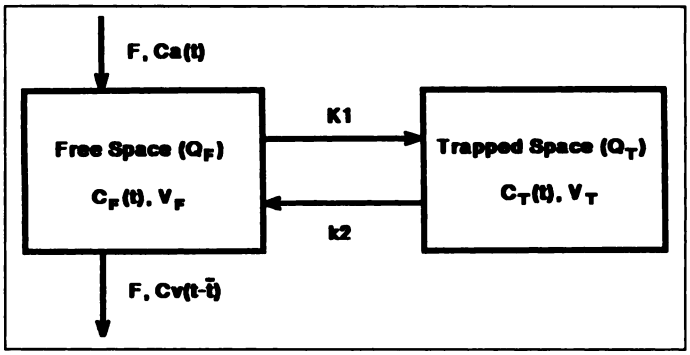

FIGURE 1. Functional two-compartment model describing myocardial kinetics of ^{13}N-ammonia and ^{82}Rb. k_1 and k_2 reflect tracer exchange tracer between free and trapped space. F = flow to region, Ca(t) = arterial concentration of tracer, Cv(t-t) = venous concentration of tracer, V_F = volume of free space with concentration and is volume of trapped space with concentration C_T.

The standard noninvasive method of measuring arterial input function uses serial, 6–10-sec, multiple (16–20) PET images that require substantial processing time and is thus not optimal for routine clinical studies. Furthermore, the short 6–10-sec images used for serial dynamic PET data acquisition are of poor quality with such poor statistical content as to preclude clinical diagnostic use. As a relatively simple, clinically applicable alternative, we tested the validity of measuring arterial input function and myocardial activity from single 0–1-min, 0–2-min and 1–2-min PET images to determine myocardial perfusion compared to compartmental models using serial 6-sec PET images and blood sampling data.

To describe the kinetic characteristics of ^{13}N-ammonia and ^{82}Rb in the myocardium, we began with a generic functional two-compartment model as previously described (*15–17*), in which the two compartments are the free and trapped space illustrated in Figure 1. V_F and V_T are volumes of free and trapped space (ml/g), respectively, with concentration $C_FT(t)$ and $C_T(t)$ (cps/ml). The kinetic transport constants k_1 (ml/min/g) and k_2 (/min) represent the forward and backward transfer rates of tracer from free to trapped space. F (ml/min/g) is myocardial flow to the region, Ca(t) arterial concentration of the tracer and Cv(t) venous concentration of the tracer (cps/ml). The total myocardial tracer concentration at time t, P(t), can be described by the following equation:

$$P(t) = V_F C_F(t) + V_T C_T(t). \qquad \text{Eq. 1}$$

P(t) can also be expressed as the integral difference between the input and output.

$$P(t) = \int_0^t FCa(x)\,dx - \int_0^t FCv(x - t)\,dx. \qquad \text{Eq. 2}$$

Extraction fraction of the tracer at time t can be expressed as the ratio of the amount of the tracer trapped to the total amount delivered.

$$E(t) = \frac{V_T C_T(t)}{F\int_0^t Ca(x)\,dx}. \qquad \text{Eq. 3}$$

From this general two-compartment model and equations, we then derived two different versions for calculating myocardial perfusion specific for both ^{82}Rb and ^{13}N-ammonia. The first version is called the Simple model because it has been simplified to one unknown,

flow, to be calculated from two observed variables, myocardial uptake and arterial input function, each measured from a single PET image acquired during the 2 min after intravenous injection of radionuclide. The second version is called the Compartmental model because it has fewer simplifying assumptions and four or five unknowns (see below) determined by curve fitting the model equations to observe myocardial and blood-pool, time-activity curves measured from multiple (16) serial PET images taken dynamically every 6–10 sec for the first 2 min after intravenous injection followed by standard frame mode acquisition.

Simple Flow Model. If the time at which the flow is measured, t, is long enough after the tracer injection, the tracer in the free space, $V_F C_F(t)$, is negligibly small compared to that trapped in the myocardium. An approximation $P(t) \approx V_T C_T$ can be made and Equation 3 can be expressed as follows:

$$F = \frac{P(t)}{E(t)\int_0^t Ca(x)\,dx}. \qquad \text{Eq. 4}$$

This equation describes the mathematical relations among flow, extraction and arterial input of the simple flow model. Schelbert et al. (*31*) measured cardiac extraction fraction of ^{13}N-ammonia in open-chest dogs using external scintillation detection after intracoronary bolus injection. Mullani et al. (*15,16*) measured cardiac extraction fraction of ^{82}Rb in open-chest dogs using external beta probes placed directly over the heart after an intravenous bolus injection of the tracer. To account for flow-dependent extraction in both the simple and two-compartment models, we used the experimentally observed relation between flow and extraction fraction given by Schelbert et al. for ^{13}N-ammonia (*31*) and by Mullani et al. for ^{82}Rb (*15,16*) during the 1 min after tracer injection over a wide range of flows. Then, we applied the Renkin-Crone model (*18–23*) to these published extraction-flow data with a new term accounting for the flow-dependent, permeability-surface area (PS) product as derived in the Appendix. We then rearranged the equations as follows (see Appendix):

$$E_N = 1 - e^{-(1.34+0.48F)/F} \qquad \text{Eq. 5}$$

$$E_R = 1 - e^{-(0.45+0.16F)/F}, \qquad \text{Eq. 6}$$

where E_N and E_R are the extraction fraction of ^{13}N-ammonia and ^{82}Rb, respectively, at 1 min after tracer injection in relation to flow, F. Substituting these equations for E into Equation 4 gives the following equations. For rubidium the simple equation becomes:

$$\text{Rubidium} \quad P(t) = F[1 - e^{-(0.45+0.16F)/F}]\int_0^t C_a(x)\,dx. \qquad \text{Eq. 7}$$

For ^{13}N-ammonia the simple equation becomes

$$\text{N-13 ammonia} \quad P(t) = F[1 - e^{-(1.34+0.48F)/F}]\int_0^t C_a(x)\,dx. \qquad \text{Eq. 8}$$

For the simple model for ^{13}N-ammonia and for ^{82}Rb, "instantaneous" myocardial activity, P (t), was measured by PET at 60 sec and the arterial input function integrated over 60 sec up to that time. It is a simple equation because there is only one unknown to be calculated, F, from measured values of P (t) and the arterial input function by PET.

These equations are derived for calculating myocardial flow at a point in time, T, based on the simple equation by dividing instantaneous myocardial counts at time, T, by the arterial input function integrated up through time T. For validating the simple model in animal studies, the shortest realistic duration of image acquisition was used, 6 sec, at 60 sec after injection for measuring myocardial uptake, P(t), to approximate as closely as possible the conditions under which the equation applies. However, the statistical count content of 6-sec PET images is not of diagnostic quality for clinical purposes, particularly for regional quantification of CFR.

PET systems typically collect counts over a longer period of time in which duration of image acquisition is inversely related to statistical noise in the image data. To reduce the statistical noise in the data, the counts are integrated for as long as possible, particularly for clinical studies where minimizing image noise is diagnostically important. Therefore, to accommodate the simple flow model to a clinical PET acquisition with better statistical content for diagnostic purposes, a further modification was made in the simple flow model as follows:

$$F = \frac{\frac{1}{(t_2 - t_1)}\int_{t_1}^{t_2} P(x)\,dx}{E\int_0^{t_2} C_a(x)\,dx}.$$

Instead of using instantaneous myocardial counts measured on a 6-sec image, an average of myocardial counts over a longer period of the data collection time from t_1 to t_2 was used to improve statistical content. An assumption made in this modified equation is that the observed myocardial counts P(t) do not change very much from time t_1 to t_2, and therefore an average value of P(t) during that interval can be obtained that approximates the instantaneous value. Experimentally, this assumption appears justified since myocardial uptake is relatively stable after the first minute.

The average of myocardial counts over the first 2 min of data after injection has less statistical noise but underestimates the counts at time, T, due to the slow increase of the myocardial counts beginning at time zero. The underestimation error can be 30%–40% if the myocardial counts are integrated from time zero through the second minute after injection. Better image quality, better statistical quantitation of instantaneous myocardial activity at 60 sec and a better estimate of blood flow for clinical purposes are obtained if the myocardial activity is integrated for 1 min starting at 1 min postinjection of tracer when myocardial uptake is more stable. The total arterial input function is collected from time zero up through the end of the data acquisition time, as is the case for determining instantaneous blood flow. The averaged or integrated myocardial counts beginning at the first minute after injection may still theoretically slightly underestimate instantaneous flow, but the error is negligible as shown subsequently.

This version of the simple model adapted for optimal clinical diagnostic image quality is called the Averaged Simple model because myocardial uptake is obtained as the average myocardial counts from a 1-min PET image (the second minute after the rise in activity after intravenous injection) as compared to the 6-sec image for instantaneous myocardial uptake.

In comparison, Nienaber et al. (*27*) used integrated arterial input and instantaneous myocardial activity by PET 60 sec after tracer injection to minimize errors due to spillover activity from the myocardium to blood pool and ^{13}N-ammonia metabolites at longer times. However, the image quality or statistical content of PET data is very poor in these short instantaneous images, whereas it is markedly improved on 1-min images obtained in the first to second minute after injection, as in our Averaged Simple model. In this

early acquisition period, these errors due to spillover and metabolites are readily corrected.

To compute absolute flow, several corrections have to be made to the data:

1. Correct the myocardial counts for partial volume (PV) losses and for spillover (S_m) from blood-pool activity to the myocardium.
2. Correct blood-pool activity or arterial input for myocardial to blood-pool spillover (S_b); correct blood-pool activity by a cross-calibration factor (CF) obtained by comparing blood-pool activity by PET to blood samples counted in a well counter and for metabolites of ^{13}N-ammonia (M) in blood not extracted by myocardium.
3. Correct both myocardial and blood-pool activity for random coincidences, physical decay and deadtime losses.

These corrections are detailed below.

Data Analysis and Partial Volume, Spillover and Metabolite Corrections. Initially acquired, raw PET data underwent standard corrections for randoms, physical decay and deadtime losses. Then, partial volume corrections were estimated theoretically and verified experimentally by imaging the Mullani partial volume phantom. The observed myocardial activity was corrected using a recovery coefficient for the myocardium (PV) of 0.73 for ^{13}N-ammonia and 0.70 for ^{82}Rb. There is also a partial volume loss from blood-pool activity that decreases arterial input function by PET. The correction factor for this error (CF) was calculated as the ratio of integrated arterial input function by counting blood samples in a well counter to that by PET and was 1.109 (CF) for ^{13}N-ammonia and 1.166 for ^{82}Rb. Spillover fractions of blood-pool activity into myocardium (S_m) were computed at 0.16 for ^{13}N-ammonia and 0.19 for ^{82}Rb, assuming a left ventricular wall thickness of 1.2 cm and knowing the positron range of the radionuclide.

The correction for metabolites, M, was taken from Rosenspire et al. (*32*) as 0.95 due to 5% of blood-pool activity being metabolites labeled with ^{13}N but not extractable by the myocardium. Since it is time-dependent, this metabolite correction for ammonia was made as a function of time of the arterial sample using an exponential function, calculated for the second minute after intravenous injection.

The simple flow equation with partial volume and corrections spillover are shown below:

$$F = \frac{\frac{1}{PV \times (t_2 - t_1)} \int_{t_1}^{t_2} \{P(x) - (S_m \times C_a(x))\}\, dx}{E(CF)\left[\int_0^{t_2} \{M \times C_a(x) - S_b \times P(x)\}\, dx\right]},$$

where the corrections PV, S_m, S_b, CF and M are defined above.

In application, myocardial uptake, E × F, is obtained by computing the ratio of the myocardial uptake to the arterial input data. This equation is represented by

$$\text{Myocardial Uptake} = F \times E = \frac{\frac{1}{PV \times (t_2 - t_1)} \int_{t_1}^{t_2} \{P(x) - (S_m \times C_a(x))\}\, dx}{(CF)\left[\int_0^{t_2} \{(M(x) \times C_a(x)) - (S_b \times P(x))\}\, dx\right]}.$$

Then, flow is calculated by substituting Equations 5 and 6 for E_N or E_R for E depending on whether ^{82}Rb or ^{13}N-ammonia is being used.

Increasing the time period over which the average myocardial count is measured further improves the image quality for quantitation of myocardial uptake by reducing image noise or statistical uncertainty. However, prolonging this period for determining myocardial counts beyond 2–3 min increases the error in the arterial input function due to spillover of activity from the myocardium into the blood pool and the error due to blood metabolites of ^{13}N-ammonia. Since the equations require that myocardial uptake and arterial input function be measured concurrently or simultaneously in time, there is an inherent trade off between the error in the arterial input function with the error in myocardial activity depending on the time period after intravenous injection when they are measured. Earlier images after injection have the most accurate arterial input data and least accurate myocardial uptake data due to larger spillover of activity from the blood pool to myocardium which has to be corrected. Later images after injection have the most accurate myocardial uptake data and least accurate arterial input data due to large spillover activity from the myocardium to blood pool and blood metabolites of ^{13}N-metabolites. The most useful compromise is the 1-min time period from the first to the second minute after intravenous injection for myocardial uptake, with arterial input integrated during these first 2 min or by obtaining a single 2-min image in list mode. These data are then used to reconstruct a single 1-min myocardial uptake image and a single 2-min arterial input image.

The data were also analyzed using functional two-compartment models derived separately for ^{13}N-ammonia (compartment model N) and for ^{82}Rb (compartment model R) by compartmental analysis and solutions for the unknowns by curve-fitting each model to observed myocardial time-activity from multiple serial PET images, as described below.

Compartmental Model R

In this model, the two compartments, free and trapped spaces, are represented by volumes V_F and V_T with concentrations of C_F and C_T, respectively. Equation 1 can be modified by substituting for V_TC_T the expression from Equation 3, the product of extraction fraction, flow and arterial input function as follows:

$$P(t) = V_FC_F(t) + E(t)F \int_0^t C_F(x)\, dx. \qquad \text{Eq. 9}$$

This general equation contains the term $V_FC_F(t)$, the amount of activity in the free space, not present in the simple equation and is therefore a more complete model but with more unknowns that must be solved by curve fitting. If the tracer is injected into the femoral veins as a bolus, CF(t) can be adequately described by convolving the arterial input function with the following equation:

$$bte^{-at},$$

where a and b are determined by curve fitting of the equations below to the observed rubidium data (*15,16*). Therefore, we convolved Ca(t) with the curve bte^{-at} to obtain $C_F(t)$.

$$C_F(t) = bte^{-at} * C_a(t), \qquad \text{Eq. 10}$$

where * is the convolution operator.

Substitution of Equation 10 into Equation 9 and using the relation between flow and extraction fraction, E_N and E_R, gives the following equations with four unknowns to be solved by fitting the model to the observed tissue time-activity curves. The four unknowns are V_F, F, a and b whose values are determined by best

fit of the equations below to the observed myocardial counts, P(t), and the arterial input function.

The general two-compartment equation is written as follows:

$$P(t) = V_F C_a(t) * bte^{-at} + E(t)F \int_0^t C_a(x) * bxe^{-ax}\,dx. \quad \text{Eq. 11}$$

Substituting E_R for E from Equation 6 into Equation 11, the two-compartment equation for rubidium becomes:

$$P(t) = V_F C_a(t) * bte^{-at} + F[1 - e^{-(0.45+0.16F)/F}] \int_0^t C_a(x) * bxe^{-ax}\,dx. \quad \text{Eq. 12}$$

To use this equation with ^{13}N-ammonia, Equation 5 for E_N is substituted for E(t) in Equation 11 and the two-compartment equation becomes:

$$P(t) = V_F C_a(t) * bet^{-at} + F[1 - e^{-(1.34+0.48F)/F}] \int_0^t C_a(x) * bxe^{-ax}\,dx. \quad \text{Eq. 13}$$

Compartmental Model N

As a comparison with previously published compartment models for ^{13}N-ammonia, we utilized the BMDP software package (Los Angeles, CA) using differential equations. For analysis by BMDP, as previously published for compartmental models for ^{13}N-ammonia, Equation 13 for ammonia above can be rewritten in differential form. For each compartment of the model N, the rate of change in the tracer concentration can be described by the following differential equations:

$$\frac{d}{dt} Q_F(t) = FC_a(t) - K_1 C_F(t) + k_2 Q_T(t) \quad \text{Eq. 14}$$

$$\frac{d}{dt} Q_T(t) = [K_1 Q_F(t)]/V_F - k_2 Q_t(t). \quad \text{Eq. 15}$$

In model N, if we assume, as have other investigators (*24,27–31*) that the venous concentration of the tracer equals tracer concentration in the free space, then Equation (*14*) can be changed into the following equation developed by Huang et al. (*24*):

$$\frac{d}{dt} Q(t) = FC_a(t) - [(K_1 + F)Q_F(t)]/V_F + k_2 Q_T(t). \quad \text{Eq. 16}$$

In model N, the value of V_f for ^{13}N-ammonia and ^{82}Rb were also fixed at 0.8 ml/g and 1.0 ml/g, respectively, as reported by Smith et al. (*30*), Krivokapich et al. (*29*) and Endo et al. (*28*). For model N, k_2 was not assumed to equal zero but was estimated since better fit of the model to observed data was observed when k_2 was finite. Therefore, in these equations there are five unknowns, R_1, k_2, F, Q_F and Q_T determined by fitting this equation to the observed uptake of radionuclide, Q, and arterial input function. Since k_2 was not assumed to be zero, this model has one additional unknown.

Blood samples counted in a well counter were used to determine arterial input function in the compartmental models to calculate myocardial blood flow as a standard reference without the errors due to blood metabolites or myocardium to blood-pool spillover. Arterial input was also determined by serial dynamic PET and by a single PET image acquired throughout the time frame to obtain myocardial uptake. For compartmental analysis, nonlinear least squares regression and numerical integration were used in the BMDP software.

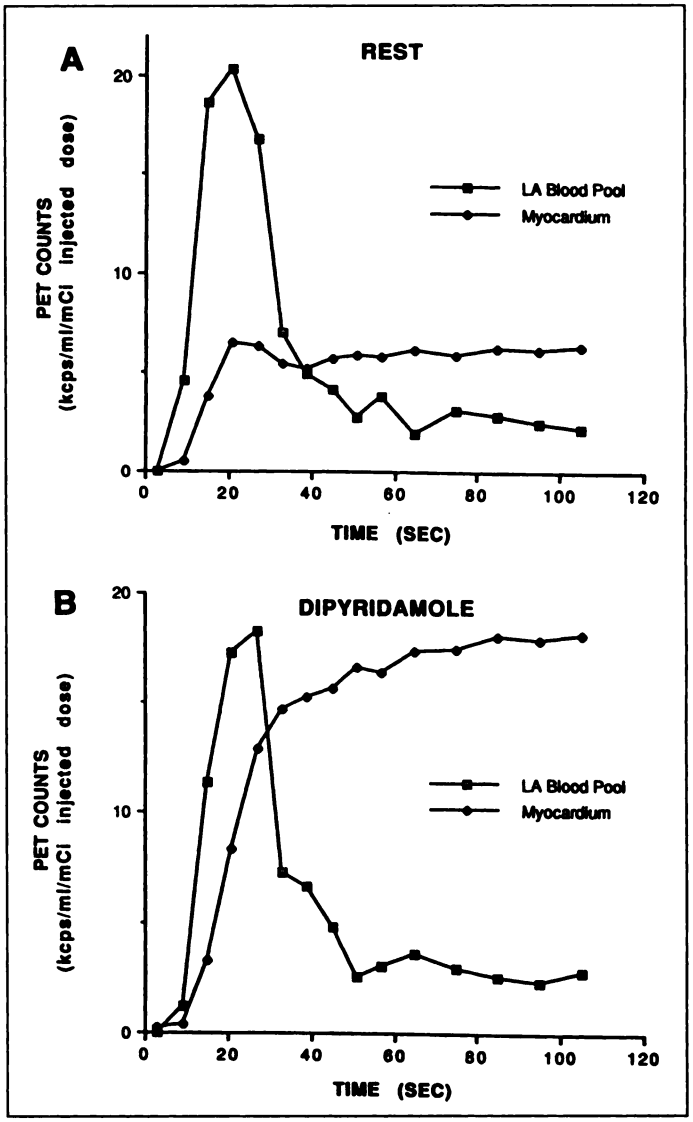

FIGURE 2. Time-activity curves for left atrial and left ventricular myocardium derived from serial PET images of ^{13}N-ammonia at rest (A) and after dipyridamole infusion (B).

The Simple models and compartmental models N and R are the three basic models for determining CFR with cationic PET radiotracers extracted by the myocardium: ^{13}N-ammonia and ^{82}Rb. We therefore compared application of all three models with both of these radionuclides to determine which model best described the kinetic behavior of each radionuclide, the differences in kinetic behavior between these radiotracers and their applicability for determining CFR for routine clinical application.

RESULTS

Figure 2 shows typical left atrial and myocardial time-activity curves obtained at rest (Fig. 2A) and after dipyridamole infusion (Fig. 2B). After dipyridamole administration, myocardial activity increased markedly. The area under the blood-pool, time-activity curve or arterial input function, was decreased after dipyridamole infusion. Similar curves were obtained for ^{82}Rb but are not shown due to space constraints.

For complete compartmental analysis, a typical curve fit of model N to the myocardial time-activity curve of ^{13}N-ammonia is shown in Figure 3A. Addition of finite k_2 values to model N eliminated residuals in the middle and late time period of the fit. Model R could not be fit to the time-activity curves of ^{13}N-ammonia. Therefore, model R was not workable with ^{13}N-ammo-

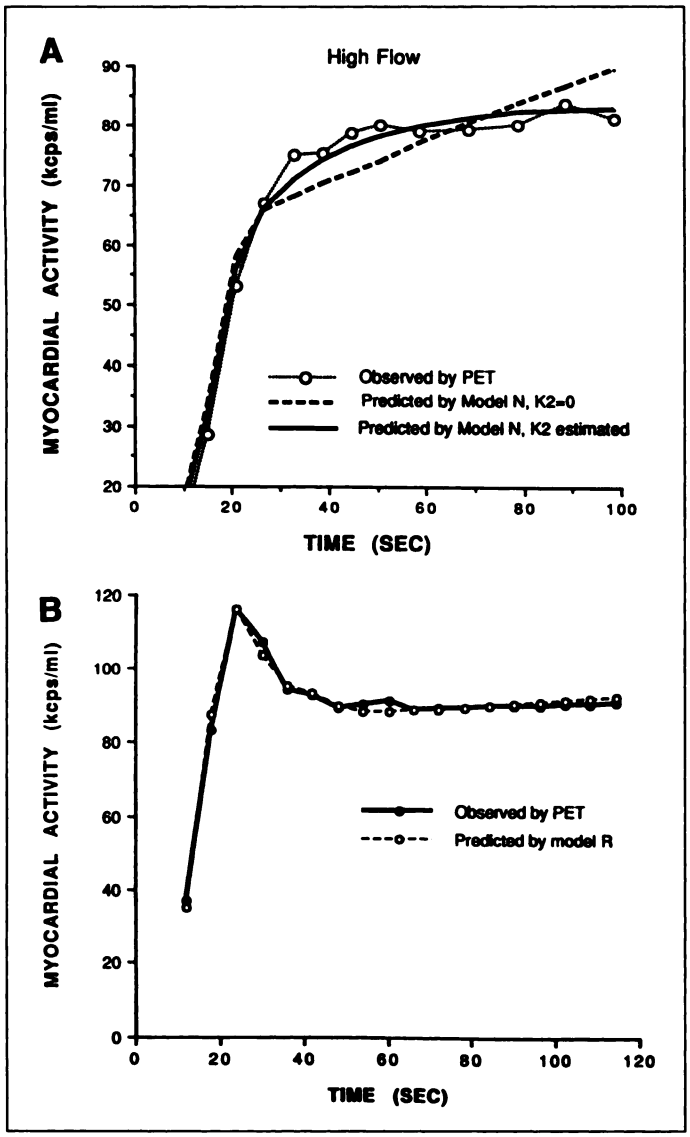

FIGURE 3. (A) Typical curve of model N fitted to the myocardial time-activity data of ^{13}N-ammonia obtained by PET at high flow after dipyridamole (A). Estimating a finite value of k_2 to optimize the model fit to observed data eliminated residual misfit in the middle and late time periods. (B) Typical curve of model R fitted to the myocardial time-activity data of ^{82}Rb obtained by PET.

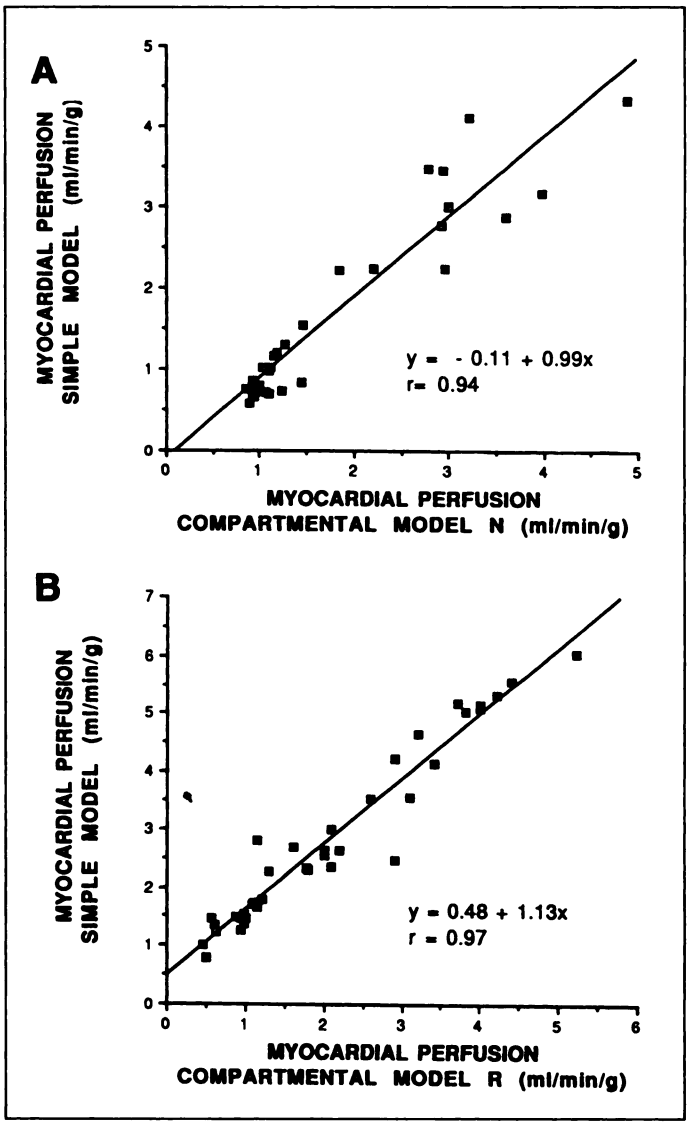

FIGURE 4. (A) Myocardial perfusion estimated by PET from ^{13}N-ammonia using the Simple model compared to the complete compartmental model N. (B) Myocardial perfusion estimated by PET from ^{82}Rb using the Simple model compared to model R.

nia, i.e., was not appropriate for or failed to describe the kinetics of ^{13}N-ammonia. A characteristic curve fit of model R to the myocardial time-activity curve of ^{82}Rb is shown in Figure 3B. The shape of the time-activity curves of these two radionuclides is quite different, reflecting different biological behavior with different models required for suitable fitting to the time-activity curves of each radionuclide obtained by PET.

Figure 4A correlates myocardial perfusion calculated from the simple model for ^{13}N-ammonia with perfusion determined by complete application of compartmental model N. There is a good correlation between these two datasets, with a correlation coefficient r = 0.94 and a slope of 0.99. Figure 4B correlates myocardial perfusion calculated from the simple model for ^{82}Rb compared to perfusion determined by complete compartmental model R. There is a good correlation with an r value of 0.97 and a slope of 1.13.

Figure 5 correlates CFR calculated from the complete compartmental model N for ^{13}N-ammonia and model R for ^{82}Rb with electromagnetic flow meter data. For ^{13}N-ammonia, CFR determined by model N correlated well with CFR by electromagnetic flow meter with r = 0.94 and slope of 0.97 (Fig. 5A). Compartmental model R could not be fit to the ^{13}N-ammonia data, and therefore the characteristics of this model did not fit ammonia kinetics. For ^{82}Rb, CFR determined from model R correlated well with CFR obtained by electromagnetic flow meter with r = 0.88 and slope = 1.13 (Fig. 5B). CFR for ^{82}Rb calculated using model N markedly underestimates CFR compared to flow meter data, indicating that model R does not describe the kinetics of ^{13}N-ammonia.

For model R, the volume of distribution of ^{82}Rb was also estimated. Figure 6 shows the relation between the distribution volume of the free space (V) for ^{82}Rb and calculated flow values (F). Linear regression yields V = 0.048 F + 0.13, r = 0.74. The mean value ± s.d. of V at rest was 0.15 ± 0.04. Thus, the volume of the free space for ^{82}Rb is about 15% of the myocardium and increases linearly as flow increases, reflecting capillary recruitment and increased capillary surface area.

Arterial Input Function and Effects of Dipyridamole

To estimate the effect of dipyridamole on arterial input function, integrated arterial input function was measured on serial blood samples, normalized to tracer injection dose and was correlated with the dose of dipyridamole (Fig. 7) for ^{13}N-ammonia and ^{82}Rb, respectively. Integrated arterial input function by well counter

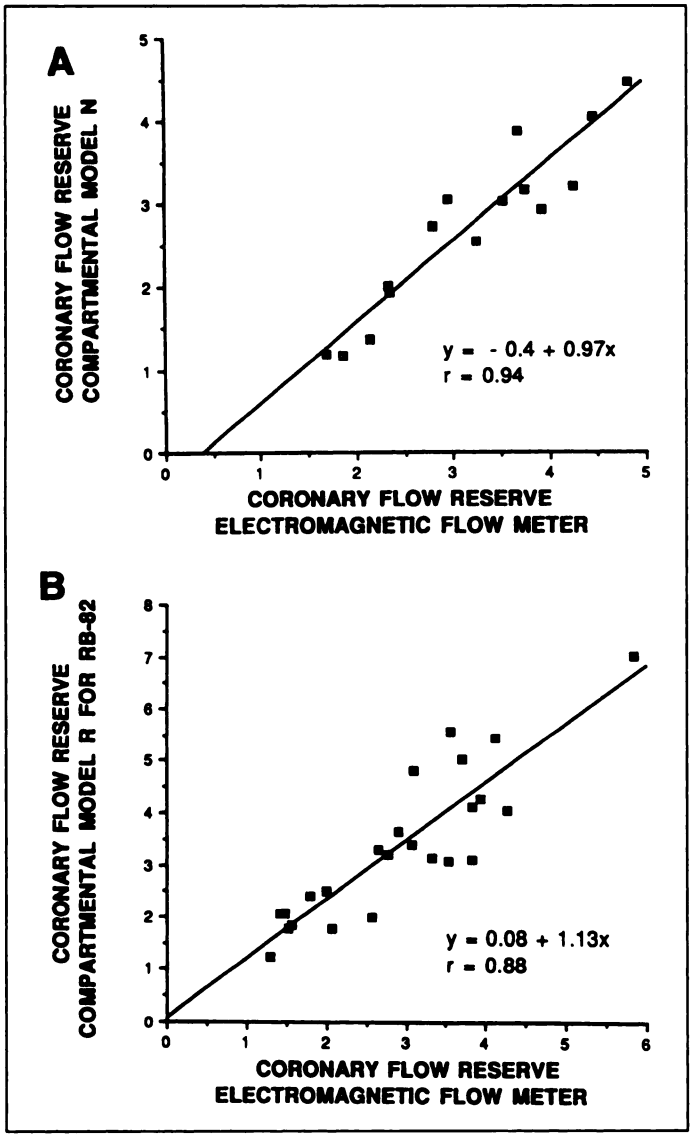

FIGURE 5. (A) CFR by PET, ^{13}N-ammonia and model N compared to CFR obtained by electromagnetic flow meter. (B) CFR by PET, ^{82}Rb and model R compared to CFR by electromagnetic flow meter.

measurements was inversely related to dipyridamole infusion dose. Therefore, dipyridamole caused a dose-dependent decrease in arterial input function of radionuclide perfusion tracers. Arterial input function determined from serial multiple 6-sec PET images over 1 min and a single 1-min PET image of first-pass blood pool correlated well with each other (r = 0.94) and with blood samples counted in a well counter (r = 0.94). However, PET underestimated integrated input function by 10.9% compared to well counter data most likely due to partial volume errors. Therefore, the PET-derived arterial input function was corrected upward by 10.9% in the Simple models.

Averaged Simple Model for Clinical Application

Both the Simple and compartmental models used instantaneous myocardial uptake measured on a 6-sec PET image to calculate flow or flow reserve. To improve statistical image quality for diagnostic clinical applications, the Simple model was further adapted to obtain myocardial uptake over a 1-min period from the end of the first 1–2 min after the rapid rise of activity after intravenous injection. Figure 8 correlates coronary flow determined by the Averaged Simple model with the complete compartment model N for ^{13}N-ammonia (Fig. 8A)

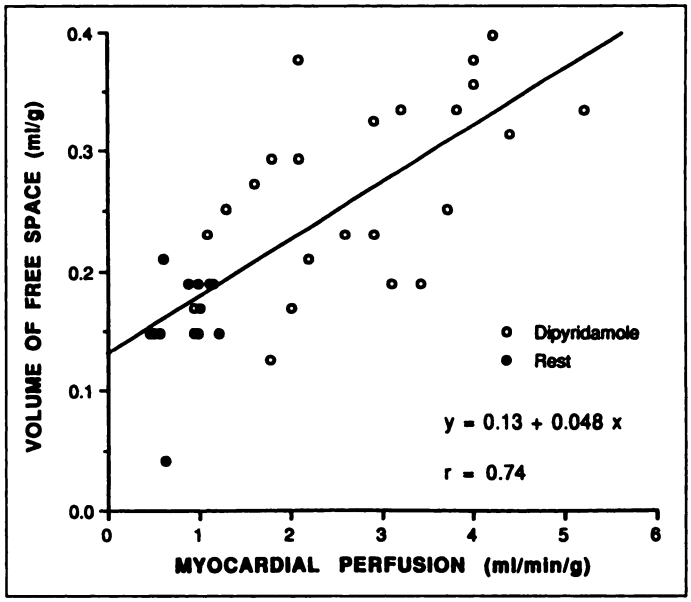

FIGURE 6. Volume of free rubidium space estimated using model R graphed as a function of myocardial perfusion up to high flows.

and model R for ^{82}Rb (Fig. 8B) with good r values and slopes near unity.

DISCUSSION

Relation of Model Compartments to Known Anatomic or Morphologic Microvascular Myocardial Spaces

Although the Simple models provide CFR measures comparable to the more complex compartmental models, the Simple models do not provide insights into the kinetic differences between these two tracers. Compartmental model R does not fit myocardial time-activity curves of ^{13}N-ammonia and compartmental model N does not fit rubidium myocardial time-activity curves of ^{82}Rb because each of the models expresses, or depends on, the specific kinetic characteristics of each tracer. Thus, compartmental kinetic models fitted by nonlinear regression to observed kinetic PET data from multiple images provide insights into the kinetics of specific tracers but do not necessarily provide better measures of CFR. For clinical applications, the Simple models accurately predict CFR and are easier to apply for routine clinical studies.

Compartmental Model R

The two-compartment kinetic model R fits myocardial time-activity curves from serial PET images of ^{82}Rb and accurately calculates myocardial perfusion and CFR. The original two-compartmental model first reported by Mullani et al. (*17*) incorporated a free space and a trapped space for describing ^{82}Rb kinetics (*15–17*). However, this original model underestimated high coronary flows (*26*) because it failed to account for the effects of capillary recruitment at high flows after dipyridamole. Our current results support the use of a more physiologically complete model that accounts for the increased capillary surface area or PS product during maximum vasodilation and has not been previously used in PET perfusion models. The average volume of the free space, V_F, estimated from model R was 0.15, increasing by 50% to 100% (Fig. 6) in association with capillary recruitment at high flows corresponding to the known size and behavior of the combined intravascular and interstitial spaces (*33–38*). Thus, maximum V_F is about twofold bigger than at rest. V_F at rest is not the same morphologically as extracellular and vascular space which are approximately 25% and 15% of the myocardium (*39*), respectively, because the

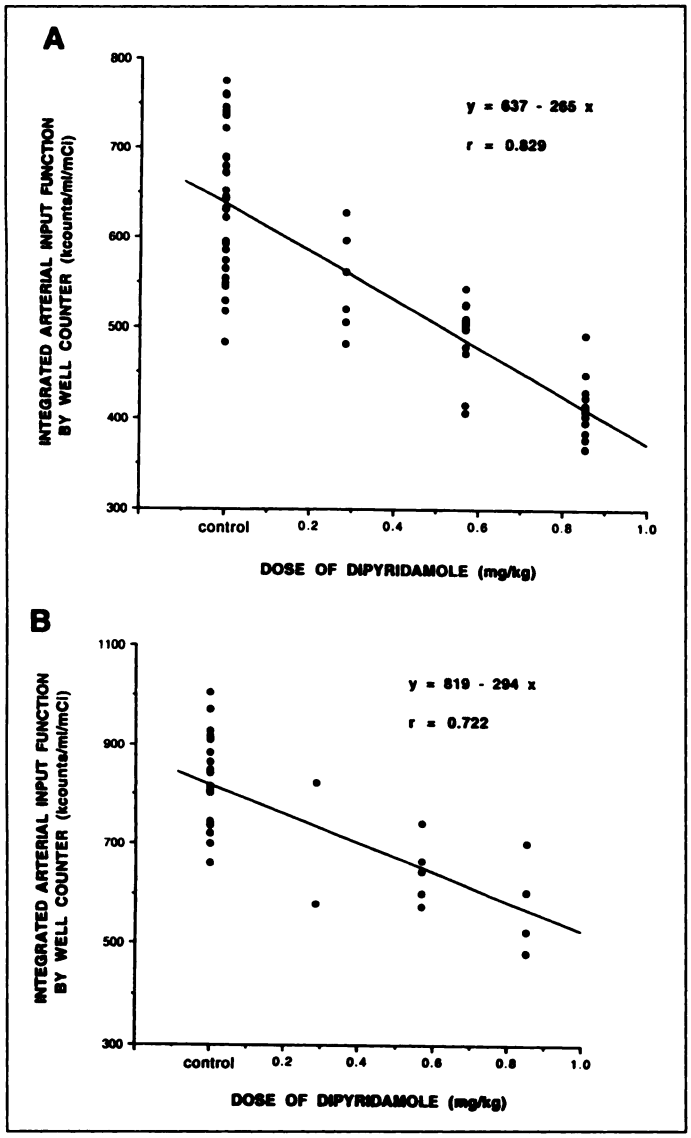

FIGURE 7. Integrated arterial input function from blood samples counted by well counter normalized to tracer injection dose graphed as a function of dipyridamole infusion dose for ^{13}N-ammonia (A) and ^{82}Rb (B).

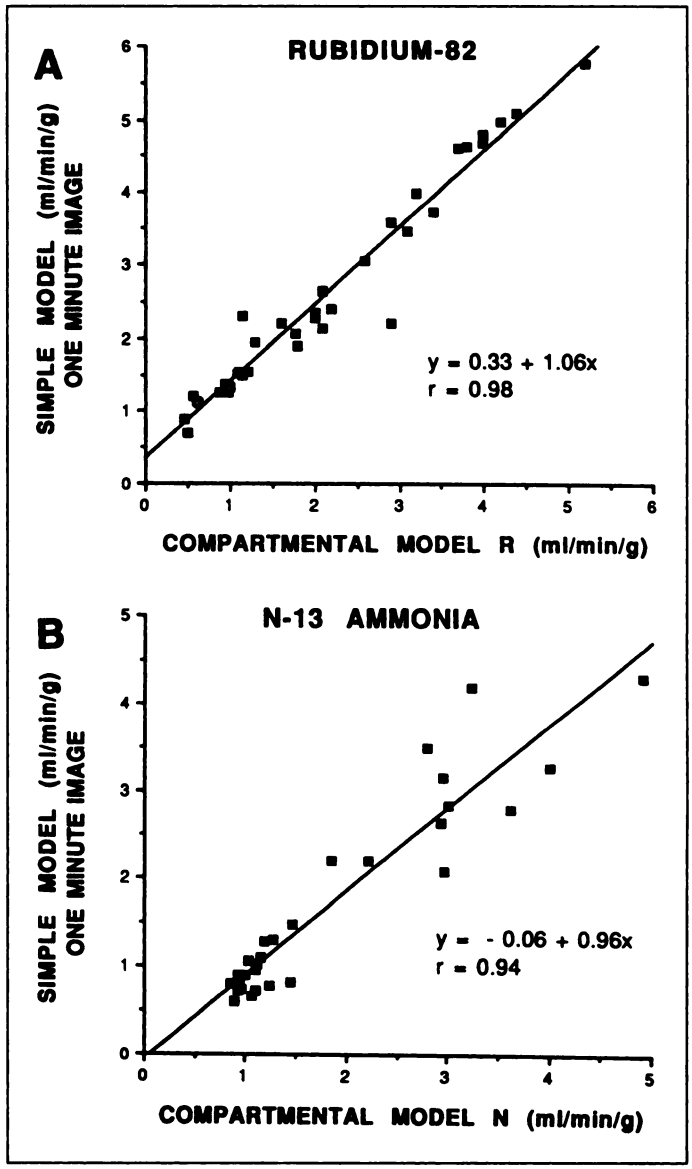

FIGURE 8. Myocardial perfusion by the Averaged Simple model using 1-min myocardial uptake data compared with perfusion obtained by model R for ^{82}Rb (A) and model N for ^{13}N-ammonia (B).

vascular endothelium offers some mild resistance to passage of rubidium and other potassium analogs. Thus, V_F at rest is a functional space of early or transient distribution without trapping that is closely related to but not identical to the vascular and interstitial spaces; V_F therefore reflects comparable changes which these morphological spaces undergo during vasodilation and recruitment.

Egress of ^{82}Rb from the cell is negligible for viable myocardium, as previously reported (*15–17,24,26,40–44*). Moreover, model R does not fit the myocardial time-activity curves from serial PET of ^{13}N-ammonia, thereby indicating different kinetic behavior of these two tracers.

Compartmental Model N

The two-compartment kinetic model N fits myocardial time-activity curves from serial PET images of ^{13}N-ammonia and also accurately determines myocardial perfusion and CFR. The volume of distribution for ^{13}N-ammonia is large, approximately 80% of the myocardial mass or 0.8 ml/g and is a fixed constant, unrelated to flow as also shown by Krivokapich et al. (*29*), Smith et al. (*30*), Endo et al. (*28*) and confirmed in our experiments. This volume of distribution is much bigger than the morphological interstitial space reported by Frank et al. (*39*). One explanation is that ^{13}N-ammonia is metabolized to products, principally glutamine, that egress slowly from the cell. In this case the volume of distribution of ^{13}N-ammonia would be large as is necessary for the compartmental model N to fit myocardial time-activity curves. The concept of a large functional volume of distribution unrelated to anatomic or morphologic microvascular space has been demonstrated by Frank et al. (*39*) using the positively charged ion, La^{+++}, which had a large volume of distribution due to binding by polyanionic extracellular structures. Similarly, for metabolically trapped tracers, the distribution volume would be larger than volume of morphologic distribution and tracer concentration in the morphologic space would be much larger than that in the apparent distribution volume.

Permeability for ^{13}N-ammonia is three times that for ^{82}Rb at all levels of flow (see Appendix), reflecting high lipid solubility. Thus, two-compartment model N for ^{13}N-ammonia is markedly different from ^{82}Rb and does not correspond to physiologic microvascular spaces but represents functional metabolic compartmentalization of ^{13}N-ammonia.

The compartmental models for ^{82}Rb and ^{13}N-ammonia accu-

rately determine CFR measured independently by electromagnetic flow meter and provide insights into their kinetics. However, their requirement for multiple serial PET scans and complex processing for compartmental analysis precludes their routine clinical application. The simple models for ^{82}Rb and ^{13}N-ammonia can be applied for routine clinical PET by obtaining 2 min of list mode data. These data are processed to reconstruct a single cumulative 2-min static image of the first-pass left ventricular blood pool as a simplified arterial input function and a single, cumulative, static 1-min image of myocardial uptake. With this Average Simple model, diagnostic quality images are obtained, myocardial perfusion and CFR are measured, multiple serial PET images are not required and processing time is markedly reduced for routine application and rapid clinical throughput. Standard diagnostic images of myocardial uptake may be obtained in profile mode over 6 min for ^{82}Rb or over 15 min for ^{13}N-ammonia after the acquisition of the flow data in the first 2 min.

Other Perfusion Radiotracers

Myocardial perfusion in cc/min/g has been measured by ^{15}O-water (*45*). However, image quality with ^{15}O-water is severely limited for diagnostic clinical imaging due to low counting statistics since it is not extracted from the myocardium and requires blood-pool subtraction. Although well documented as a measure of myocardial perfusion in investigative protocols (*45*), poor diagnostic quality images have limited the clinical use of ^{15}O-water. For this reason, there are no published reports on its diagnostic sensitivity and specificity for detecting coronary artery disease. Moreover, quantifying myocardial perfusion by ^{13}N-ammonia has been shown to be equivalent to ^{15}O-water but with better quality diagnostic images (*46*).

Effects of Dipyridamole on Arterial Input Function

Assessing CFR by PET requires imaging at rest and after intravenous administration of dipyridamole. Since dipyridamole increases cardiac output, there is a dose-related decrease in arterial input function after dipyridamole. Cardiac output (CO), tracer injection dose and arterial input function have the following relation based on an indicator dilution method (Henriques-Hamilton Principle):

$$CO = \frac{\text{Inj. Dose}}{\int_0^\infty C(t)\,dt}.$$

In their pioneering studies of rubidium in 1967, Knoebel et al. (*47*) applied this principle for measuring global myocardial perfusion and cardiac output using a two-detector coincidence counting system with ^{84}Rb-Cl. She reported that dipyridamole infusion increases cardiac output by approximately 34%. Consistent with her study results 26 yr earlier, our quantitative PET data demonstrate a 27% ± 9.8% decrease in arterial input function after dipyridamole, which varies inversely with dose. Our results validate generator-produced ^{82}Rb for quantifying regional CFR with routine clinical PET.

Timing of PET Data Acquisition for Arterial Input Function and Myocardial Tracer Uptake

Different optimal times for PET data acquisition for measuring blood-pool (arterial input function) and myocardial uptake create tradeoffs that are important for accurate measuring of perfusion and CFR. Table 1 summarizes these tradeoffs by showing the effects of various data acquisition timing protocols on arterial input, myocardial uptake, image quality, timing concurrence, measurement of CFR and clinical applicability.

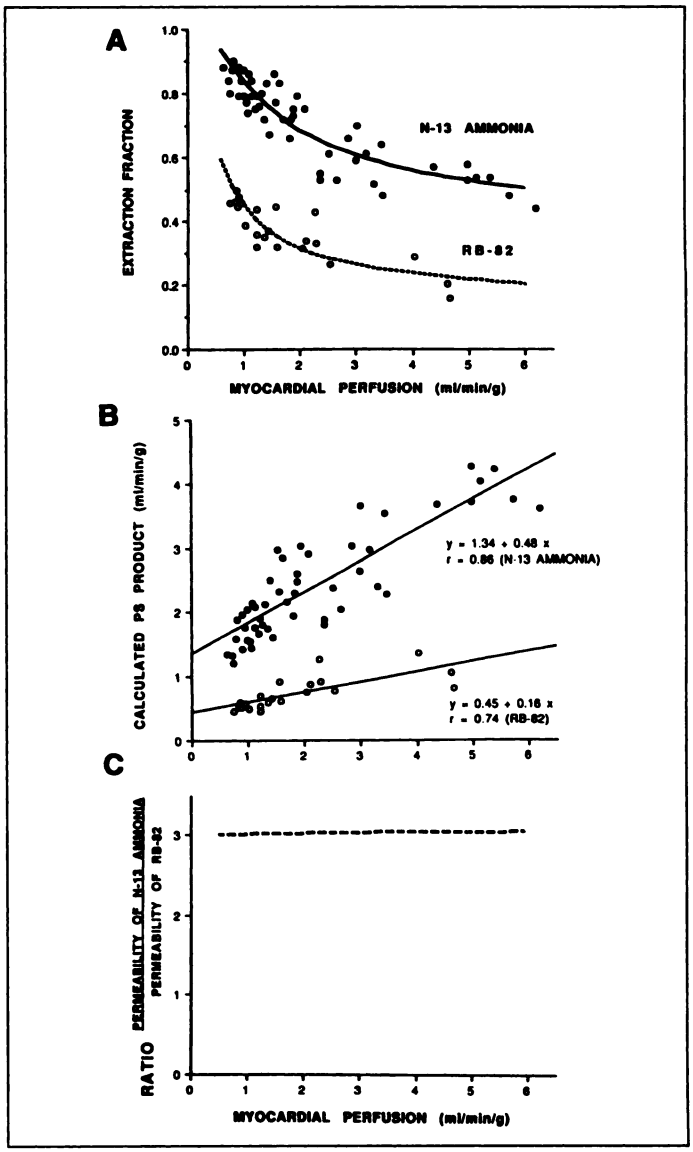

FIGURE 9. (A) Extraction fraction of ^{13}N-ammonia and ^{82}Rb recalculated from the data of Schelbert et al. (*3*) and Mullani et al. (*15,16*) as a nonlinear function of myocardial blood flow. (B) Estimated PS product (permeability × surface area) of ^{13}N-ammonia and ^{82}Rb from the data of Schelbert et al. (*31*) and Mullani et al. (*15,16*) as a function of myocardial blood flow. (C) Ratio of the permeability of ^{13}N-ammonia to that of ^{82}Rb as a function of myocardial blood flow.

On early images (0–1 min after intravenous injection), blood-pool activity is optimally measured but myocardial uptake is subject to a large error due to spillover of activity from the blood-pool to myocardial regions of interest. On later images (2–3 min after intravenous injection) myocardial uptake is optimally measured, but blood-pool activity is subject to large errors due to spillover of myocardial activity into blood-pool regions of interest. Since blood-pool activity for arterial input function must be measured concurrently with myocardial activity, there is a tradeoff among these spillover errors and statistical image quality with an optimal period from the first to the second minute.

In Table 1, option A, 6-sec serial images are of such poor image quality as to preclude diagnostic usefulness. Options B,C, with 6–10-sec instantaneous uptake images, suffer the same limitation despite good arterial input data. In option E, quantitation of myocardial uptake is poor due to a larger error caused by spillover activity from intense blood-pool activity into myocardial regions of interest. In option F, quantitation of

TABLE 1
Timing of PET Data Acquisition

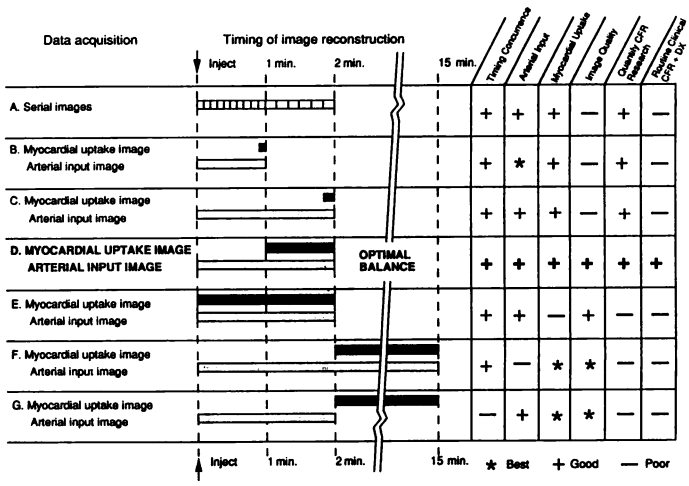

arterial input is poor due to a large error of spillover activity from myocardium into the blood-pool region of interest. Option G is unsatisfactory for quantifying flow due to nonconcurrence of arterial input and myocardial uptake data. The timing for optimal balance of the essential characteristics of quantitative clinical PET are shown in option D and by the highlighted (+) sign for each image characteristic needed.

Rubidium-82 and Finite k2 with Necrosis

In areas of myocardial necrosis, the model is not applicable because egress or backdiffusion of ^{82}Rb occurs with failure of the myocardium to trap ^{82}Rb, as first reported by this laboratory (*40–44*) and confirmed by others (*26,48,49*). Myocardial washout of ^{82}Rb is a marker of necrosis, comparable to metabolic imaging of [^{18}F]fluorodeoxyglucose (*43–44*). Therefore, areas of myocardial necrosis may be readily identified by a two-image sequence of rubidium washout and can be excluded from the analysis by the simple perfusion models which assume k_2 is zero.

CONCLUSION

Our results indicate that myocardial perfusion and CFR can be measured noninvasively by PET using either generator-produced ^{82}Rb or cyclotron-produced ^{13}N-ammonia and a simple model of transport kinetics specific for each radiotracer accounting for arterial input, flow-dependent extraction, increased PS product associated with capillary recruitment and altered arterial input function at maximum flows after high-dose dipyridamole. This simple approach acquires data in list mode over 2 min after intravenous injection. From these data, a single image of myocardial uptake and a single image of arterial input function is reconstructed. It therefore has the advantage of simplicity for routine application compared to compartmental analysis using multiple serial PET images. These models utilize a previously observed empirical relation between flow and extraction determined experimentally and applied clinically as in previously reported models.

Although ^{82}Rb and ^{13}N-ammonia are both cationic perfusion radiotracers, they demonstrate markedly different kinetics requiring different flow models. Rubidium behaves like potassium with limited permeability and low k_1 values for inward transport compared to ^{13}N-ammonia, no egress from viable myocardium ($k_2 = 0$) and distribution compartments that reflect behavior of known intravascular and interstitial microvascular spaces. By comparison, ^{13}N-ammonia behaves like a lipid-soluble, metabolically trapped radionuclide with permeability three times greater than ^{82}Rb and a large distribution volume that is much larger than known intravascular and interstitial microvascular spaces.

With increasing recognition of diffuse and/or multistenosis coronary artery disease not quantifiable by standard arteriography or conventional exercise imaging, quantitative measures of CFR by PET may provide important, clinically useful information for detecting or assessing severity of coronary artery disease.

APPENDIX

Extraction Fraction of Nitrogen-13-Ammonia and Rubidium-82

The single-capillary Renkin Crone model (*18–23*) describes the relation between myocardial extraction, flow and the PS product (permeability × surface area) by the following equation:

$$E = 1 - e^{-PS/F} \text{ or } PS = -F \ln (1 - E). \quad \text{Eq. A1}$$

Both Huang et al. (*24*) and Herrero et al. (*26*) found that this simple model did not fit their in vivo data for a constant value of PS over a wide range of coronary flows. Accordingly, we hypothesized that at high coronary flows, capillary recruitment occurs (*36–38*) so that the PS product is not a constant but is flow dependent in a multicapillary system. We therefore reanalyzed our prior data from Mullani et al. (*15*), Goldstein (*16*) and Schelbert et al. (*31*) using flow independently determined by radiolabeled microspheres, extraction measured by epicardial detectors as previously described (*15*), and we calculated PS product over a range of flows in experimental animals. From these data, the relation of extraction to flow is shown in Figure 9A and of PS product to flow in Figure 9B for both ^{13}N-ammonia and ^{82}Rb. These data show a simple linear correlation as follows:

$$PS = 1.34 + 0.48 \times F(^{13}\text{N-ammonia}) \quad \text{Eq. A2}$$

$$PS = 0.45 + 0.16 \times F(^{82}\text{Rb}). \quad \text{Eq. A3}$$

Therefore, an adapted Renkin-Crone model for a multicapillary coronary vascular bed with recruitment at high flows is more accurately described by an expression which includes the relation between PS product and flow as follows:

$$PS = PS' + sF,$$

where PS' is the resting PS product, PS is the product at any other flow level, s is the slope of the experimentally observed, linear relation between PS product and flow, F. The Renkin-Crone equation can therefore be rewritten as:

$$E = 1 - e^{(PS/F)-s}$$

$$E = 1 - e\left(\frac{PS + sF}{F}\right). \quad \text{Eq. A4}$$

The values of PS' and s were determined from the experimental data of Mullani et al. (*15*), Goldstein et al. (*16*) and Schelbert (*31*) to find expressions for extraction rubidium, E_R and ^{13}N-ammonia, E_N.

By substituting Equations 2 or 3 into Equation 1, equations for extraction fraction, taking into account the flow-dependent PS product, can be expressed as follows with the adapted Renkin-Crone (*18–23*) model:

$$E_N = 1 - e^{-(1.34+0.48F)/F} \ (^{13}\text{N-ammonia}) \quad \text{Eq. A5}$$

$$E_R = 1 - e^{-(0.45+0.16F)/F} \ (^{82}\text{Rb}). \quad \text{Eq. A6}$$

From Equations 2 and 3, the PS products for ^{13}N-ammonia and ^{82}Rb are approximately 1.8 and 0.6 ml/min/g at a flow of 1

ml/min/g. Assuming a value from the literature for S of 500/g myocardium (*21,36–38*), Equations 2 and 3 predict values of permeability, P, for ^{13}N-ammonia and for ^{82}Rb of 6×10^{-5} and 2×10^{-5} cm/sec, respectively. NH_4^+ and Rb^+ are monovalent cations with a radius size almost identical to that of K^+(1.45 A). Therefore, traditionally, NH_4^+ and Rb^+ are considered analogs of potassium, K^+, where the capillary permeability, P, for K^t is on the order of 10^{-5} cm/sec. On the other hand, NH_3 is lipid-soluble and penetrates the cell membrane chiefly by passive diffusion. Permeability, P, for NH_3 is on the order of 10^{-2} to 10^{-3} cm/sec (*21,36–38*). Although more than 95% of the total ammonia in blood is in the form for NH_4^+, the exchange of NH_4^+ with NH_3 is virtually instantaneous and not rate-limiting, thereby making ammonia behave as a lipid- and water-soluble radiotracer. Consistent with this behavior, in our data, permeability, P, of ^{13}N-ammonia is approximately three times bigger than that of ^{82}Rb (Fig. 9C) and constant for low and high flows.

ACKNOWLEDGMENTS

We are indebted to Veronica Pina, DVM, for superb surgical skills, to Patsy Kleypas for administrative support and to Ro Edens for enlightened administrative support. Supported in part by National Institutes of Health grants RO1-HL26862, HL-26885 and HL-28356.

REFERENCES

1. Gould KL, Kirkeeide RL, Buchi M. Coronary flow reserve as a physiologic measure of stenosis severity. *J Am Coll Cardiol* 1990;15:459–474.
2. Gould KL. *Coronary artery stenosis: a textbook of coronary pathophysiology, stenosis fluid dynamics, quantitative coronary arteriography and cardiac PET.* New York: Elsevier; 1991:139–168.
3. Seiler C, Kirkeeide RL, Gould KL. Basic structure-function of the epicardial coronary vascular tree–the basis of quantitative coronary arteriography for diffuse coronary artery disease. *Circulation* 1992;85:1987–2003.
4. Seiler C, Kirkeeide RL, Gould KL. Measurement from arteriograms of regional myocardial bed size distal to any point in the coronary arterial tree for assessing anatomic area at risk. *J Am Coll Cardiol* 1993;21:783–797.
5. Mintz GS, Painter JA, Pichard AD, Kent KM, et al. Atherosclerosis in angiographically "normal" coronary artery references segments: an intravascular ultrasound study with clinical corrections. *J Am Coll Cardiol* 1995;25:1479–1485.
6. Gould KL. Clinical cardiac positron emission tomography: state of the art. *Circulation* 1991;84:I22-I36.
7. Gould KL. Reversal of coronary atherosclerosis, clinical promise as the basis for noninvasive mangement of coronary artery disease. *Circulation* 1994;90:1558–1571.
8. Gould KL, Martucci JP, Goldberg DI, et al. Short-term cholesterol lowering decreases size and severity of perfusion abnormalities by positron emission tomography after dipyridamole in patients with coronary artery disease, a potential noninvasive marker of healing coronary endothelium. *Circulation* 1994;89:1530–1538.
9. Gould KL, Ornish D, Scherwitz L, et al. Changes in myocardial perfusion abnormalities by PET after long-term intense risk factor modification. *JAMA* 1995;274:894–901.
10. McGinn AL, White CW, Wilson RF. Interstudy variability of coronary flow reserve. *Circulation* 1990;81:1319–1330.
11. Wilson RF. Assessment of the human coronary circulation using a coronary Doppler catheter. *Am J Cardiol* 1991;67:44D–56D.
12. Gould KL, Goldstein RA, Mullani NA, et al. Noninvasive assessment of coronary stenoses by myocardial perfusion imaging during pharmacologic coronary vasodilation. VIII. Clinical feasibility of positron cardiac imaging with a cyclotron using generator produced rubidium-82. *J Am Coll Cardiol* 1986;7:775–789.
13. Demer LL, Gould KL, Goldstein RA, et al. Asssessment of coronary artery disease severity by positron emission tomography: comparison to quantitative arteriography in 193 patients. *Circulation* 1989;79:825–835.
14. Mullani NA, Ficke DC, Hartz R, Markham J, Wong WH. System design of fast PET scanners utilizing time-of-flight. *IEEE Trans Nucl Sci* 1981;NS-28:104–108.
15. Mullani NA, Goldstein RA, Gould KL, et al. Myocardial perfusion with rubidium-82. I. Measurement of extraction fraction and flow with external detectors. *J Nucl Med* 1983;24:898–906.
16. Goldstein RA, Mullani NA, Fisher D, Marani S, Gould KL, O'Brien HA. Myocardial perfusion with rubidium-82. II. The effects of metabolic and pharmacologic interventions. *J Nucl Med* 1983;24:907–915.
17. Mullani NA, Gould KL. First-pass measurements of regional blood flow with external detectors. *J Nucl Med* 1983;24:577–581.
18. Renkin EM. Transport of potassium-42 from blood to tissue in isolated mammalian skeletal muscles. *Am J Physiol* 1959;197:1205–1210.
19. Crone C. The permeability of capillaries in various organs as determined by use of the 'Indicator Diffusion' method. *Acta Physiol Scand* 1963;58:292–305.
20. Sheehan RM, Renkin EM. Capillary, interstitial and cell membane barriers to blood tissue transport of potassium and rubidium in mammalian skeletal muscle. *Circ Res* 1972;30:588–607.
21. Crone C, Levitt DG. Capillary permeability to small solutes. In: Renkin EM, ed. *Handbook of physiology: the cardiovascular system IV.* Bethesda, MD: American Physiological Society; 1984:411–466.
22. Ziegler WH, Goresky CA. Transcapillary exchange of the working left ventricle of the dog. *Circ Res* 1971;29:181–207.
23. Ziegler WH, Goresky CA. Kinetics of rubidium uptake in the working dog heart. *Circ Res* 1971;29:208–220.
24. Huang SC, Williams BA, Krivokapich J, Araujo L, Phelps ME, Schelbert HR. Rabbit myocardial kinetics and a compartmental model for blood flow estimation. *Am J Physiol* 1989;256:H1156–H1164.
25. Bellina CR, Parodi O, Camici P, et al. Simultaneous in vitro and in vivo validation of nitrogen-13-ammonia for the assessment of regional myocardial blood flow. *J Nucl Med* 1990;31:1335–1343.
26. Herrero P, Markham J, Shelton ME, Weinheimer CJ, Bergmann SR. Noninvasive quantification of regional myocardial perfusion with rubidium-82 and positron emission tomography. Exploration of a mathematical model. *Circulation* 1990;82: 1377–1386.
27. Nienaber CA, Ratib O, Gambhir SS, Krivokapich J, Huang SC, Phelps ME, Schelbert HR. A quantitative index of regional blood flow in canine myocardium derived noninvasively with ^{13}N-ammonia and dynamic positron emission tomography. *J Am Coll Cardiol* 1991;17:260–269.
28. Endo M, Yoshida K, Iinuma TA, et al. Noninvasive quantification of regional myocardial blood flow and ammonia extraction fraction using nitrogen-13-ammonia and positron emission tomography. *Ann Nuklearmedizin* 1987;1:1–6.
29. Krivokapich J, Keen RE, Phelps ME, Shine KI, Barrio JR. Effects of anoxia on kinetics of [^{13}N] glutamate and $^{13}NH_3$ metabolism in rabbit myocardium. *Circ Res* 1987;60: 505–516.
30. Smith GT, Huang SC, Nienaber CA, Krivokapich J, Schwaiger M, Schelbert HR. Noninvasive quantification of regional myocardial blood flow with ^{13}N-ammonia and dynamic PET. *J Nucl Med* 1988;29:950.
31. Schelbert HR, Phelps ME, Huang SC, MacDonald NS, Hansen H, Selin C, Kuhl DE. Nitrogen-13-ammonia as an indicator of myocardial blood flow. *Circulation* 1981;63: 1259–1272.
32. Rosenspire KC, Schwaiger M, Mangner TJ, Hutchins GD, Sutorik A, Kuhl DE. Metabolic fate of [^{13}N]ammonia in human and canine blood. *J Nucl Med* 1990;31: 163–167.
33. Duran WN, Marsicano TH, Anderson RW. Influence of maximal vasodilation on glucose and sodium blood-tissue transport in canine heart. *Microvasc Res* 1973;6:347–359.
34. L'Abbate A, Mildenberger RR, Zborowska-Sluis DT, Klassen GA. Myocardial tissue recruitment in the dog as determined by double tracer dilution method. *Circ Res* 1976;39:276–281.
35. Rose CP, Goresky CA, Belanger P, Chen MJ. Effect of vasodilation and flow rate on capillary permeability surface produce and interstitial space size in the coronary circulation. *Circ Res* 1980;47:312–328.
36. Martini J, Honig CR. Direct measurement of intercapillary distance in beating rat heart in situ under various conditions of 0_2 supply. *Microvasc Res* 1969;1:244–256.
37. Bassingthwaighte JB, Yipintsoi T, Harvey RB. Microvasculature of the dog left ventricular myocardium. *Microvasc Res* 1974;7:229–249.
38. Knepper MA, Packer R, Good DW. Ammonium transport in the kidney. *Phys Rev* 1989;69:179–249.
39. Frank JS, Langer GA. The myocardial interstitium: Its structure and its role in ionic exchange. *J Cell Biol* 1974;60:586–601.
40. Goldstein RA. Kinetics of rubidium-82 after coronary occlusion and reperfusion. *J Clin Invest* 1985;75:1131–1137.
41. Goldstein RA. Rubidium-82 kinetics after coronary occlusion: temporal relation of net myocardial accumulation and viability in open chest dogs. *J Nucl Med* 1986;27:1456–1461.
42. Goldstein RA, Mullani NA, Wong WH, et al. Positron imaging of myocardial infarction with rubidium-82. *J Nucl Med* 1986; 27:1824–1829.
43. Gould KL, Yoshida K, Haynie M, Hess MJ, Mullani NA, Smalling RW. Myocardial metabolism of fluorodeoxyglucose compared to cell membrane integrity for the potassium analog ^{82}Rb for assessing viability and infarct size in man by PET. *Nuklearmedizin* 1991;32:1–9.
44. Yoshida K, Gould, KL. Quantitative relation of myocardial infarct size and myocardial viability by positron emission tomography to left ventricular ejection fraction and 3-yr mortality with and without revascularization. *J Am Coll Cardiol* 1993;22:984–997.
45. Bergmann SR, Herrero P, Markham J, Weinheimer CJ, Walsh MN. Noninvasive quantification of myocardial blood flow in human subjects with oxygen-15-labeled water and positron emission tomography. *J Am Coll Cardiol* 1989;14:639–652.
46. Nitzsche EU, Choi Y, Czernin J, Hoh CK, Huang SC, Schelbert HR. Noninvasive quantification of myocardial blood flow in humans: a direct comparison of the ^{13}N-ammonia and the ^{15}O-water technique. *Circulation* 1995:in press.
47. Knobel SB, McHenry PL, Stein L, Sonel A. Myocardial blood flow in man as measured by a coincidence counting system and a single bolus of Cl. *Circulation* 1967;36:187–196.
48. vom Dahl J, Muzik O, Wolfe E, Schwaiger M. Myocardial rubidium-82 tissue kinetics assessed by dynamic position emission tomagraphy as a marker of myocardial cell membrane integrity and viability. *Circulation* 1996;93:238–245.
49. Arai M, Links JM, Takatsu H, Becker LC. Regional ^{82}Rb washout assessed by PET reflects the severity and time course of myocardial ischemia-reperfusion injury [Abstract]. *J Am Coll Cardiol* 1993;21:460A.